Corrosion Impact on mechanical properties of AA6061-T6 under Friction Stir Welding process

Kasim Mohammed Jawad

***Abstract*-**The technology of friction stir welding (FSW) has been developed about four decades ago as a very effective tool to replace the old fashion welding technique for certain alloys such as aluminum and magnesium alloys. Despite the effectiveness of FSW, there are very important challenges and difficulties for applying this technique mainly due to corrosion and erosion. In this report, the corrosion of the nugget zone area was thoroughly studied by showing microstructure, hardness, and the corrosion of AA6061-T6 alloy. A series of experiments were carried out using the same corrosive solution but the exposure corrosion time was taken after 24, 48, 72, and 96 h. areas of 200, 400, and 600 mm^2, and slurry speed of 1, 2, and 3 m/s. The results have shown that the exposure time of 48 h was the most effective time while the slurry speed of 2 m/s was the most effective speed. The hardness of the AA6061-T6 has shown very close symmetric feature on the two sides of the sample. The unique results of exposure corrosion time of 48 h and the slurry speed of 2 m/s could be considered as a good guide for future work of corrosion-erosion of aluminum and other alloys.

Keywords: AA6061-T6, Corrosion, FSW, Hardness.

I. Introduction

The lightweight, durability, and mechanical strength are among some basic properties that made the aluminum alloys including AA6061-T6 as an excellent candidate for industrial applications in manufacturing automobiles, ships, and aerospace industries [1]. Alloys such as Al, Zn, Mg, or Cu are characterized by their compact single crystal structures [2]. The plastic deformation properties are tightly related to hot deformation behavior of these alloys. Regarding the hot deformation behavior, a number of studies have been focusing on the flow stress curves for each of these alloys [3]. For aluminum alloys, it was found that the peak flow stress curves decrease as the temperature increases while the peak decreases with the stress [4]. The peak behavior was used for optimizing and estimating the thermal deformation mechanisms of aluminum alloys [5], [6]. The traditional fusion welding causes residual stress, cracks due to heat, zone melting, and porous zones [7].

This work is supported by the Middle Technical University/Institute of Technology, Baghdad, Iraq. K. M. Jawad has been employed by the Technical University since his graduation from Belgrade University in 1985.

These factors result in hindering the use of aluminum alloys in some industries such as aerospace and automobiles. Hence, using friction stir welding (FSW) has been widely considered as the best alternative to the conventional fusion welding not only for aluminum but also for other mineral alloys [8].

The Al alloys suffer from grain refinement during FSW process which causes mechanical association that naturally leads to microstructure evolution [9]. It is also noted that the formation of equiaxed grain mainly depends on recrystallization in the nugget zone (NZ) and secondly on the strong local texture which is a normal outcome of stir welding process which, eventually, deteriorates the tensile mechanical properties [10]. There is a numerous number of published articles and reviews on major alloys, however, aluminum alloys have received very good part of the articles and reviews papers due to the importance of the aluminum over other metal alloys [11]. In addition to discussing FSW, the types of the FSW tools were reviewed also [12]-[14]. The research was structure as follows: mechanism of FSW, description of FSW, materials and experiments, conclusion and future challenges, and the references.

II. Mechanism of FSW

In the last four decades since the implementation of FSW, joining aluminum pieces together was the first challenging attempt of this new technology [15]. At specific times during that period, FSW implementation was extended to other metals including steel, magnesium, copper, and light metals –the move that showed clearly the possibility of replacing the conventional fusion welding. There were at least three reasons behind shifting from conventional fusion welding to FSW: no need to melt the two pieces, environmentally friendly [16], and at very reasonable processing and cost.

As shown in Fig. 1, FSW has an advancing side (AS) and retreating side (RS). The AS part combines collinearly the speed vector and the

rotational speed where the two speeds are being parallel or antiparallel. The mechanism of FSW includes moving at tilt angle the non-consumable rotating pin into the faying surface where the two surface is to be joined together. This mechanism assisted by the collinear motion provides an effective way create very strong plastic deformation combined with very complicated mixing process around the rotation axis [17]. The welded are compromises three distinct zones: the flow transition zone, the stir zone, and the torsion zone [18].

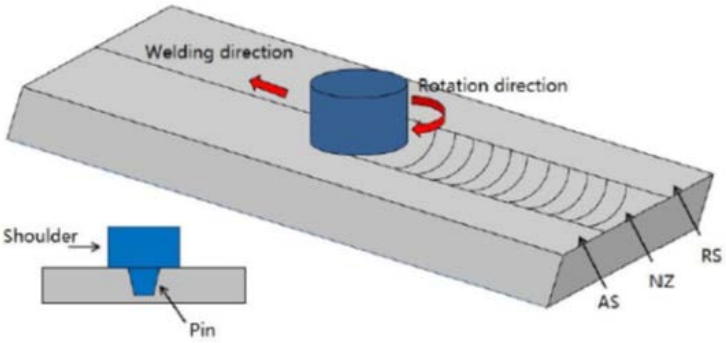

Fig. 1 FSW schematic illustration with advancing side (AS), nugget zone (NZ), and retreating side (RS) [15]

There are three motions of the metal underneath the pin tool that characterize the welding process as explained in Fig. 2. The first one is caused by the friction of the shoulder which forces the metal underneath the threaded pin tool towards it. The second motion is the movement of the metal underneath the pin tool downwards along the pin surface. The last motion is to force the metal accumulated at the pin tip to move outwards and inwards due to the helical rotational path. The repeating of these three of the metal, the stir zone is formulated expressing an onion ring structure. In some other cases, the metal flow motion varies depending on the geometrical shape of the pin. These geometrical shapes include cylindrical pin tool without screw where the third motion (downward) is omitted and a simple extrusion of the metal is created [19]. In this case, there is an insufficient deformation of material causing no clear recognition to the stir zone [20]. In the case of a flat pin tool, the stir zone shows more effective mixing [14].

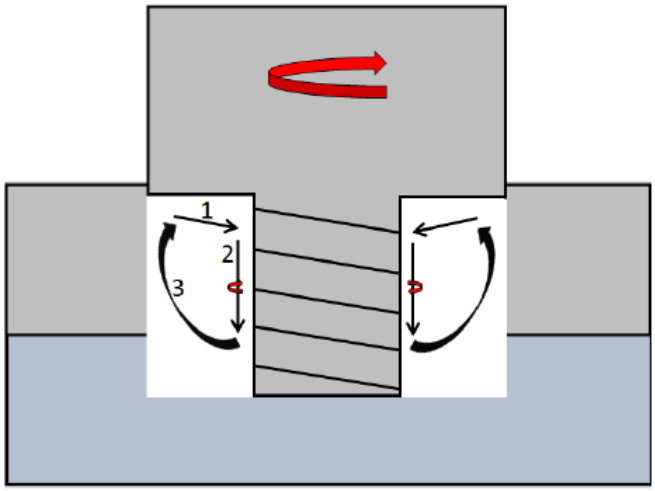

Fig. 2 Schematic illustration of material flow during FSW [15]

The solid phase bonding between the two pieces is not achieved by only developing severe plastic deformation but also due to the heat caused by the friction which causes metal flowing [21]. The frictional heat is optimized by fixing the angle of the tool at a smallest possible value which finally leads to form a metallurgical bonding between the two pieces of metal. The accuracy of measuring the temperature physically at the location of stirring is very difficult, hence finite element analysis is used to estimate the temperature distribution during the process of FSW [22]. However, it was found that the temperature depends on several factors such as holding time, rotational and transverse speed, and the angle of the tip tool. The number of factors that

affects the temperature is not agreeable amongst researchers such as the welding speed [23] or the plastic strain and the friction at the shoulder of the two pieces [24]. The average power, q, is given by (1):

$$q = \frac{2\pi}{3}\mu p \omega R_s^3 \quad (1)$$

where μ is the coefficient of friction at the stir location, p is the pressure, ω is the angular velocity, and R_s is the radius of the tool shoulder. In addition, it was also denoted that for a suitable amount of q, a fine and dynamic recrystallized grains are formed at stir zone [25] while at high values of q, the grains are coarsening. At the normal conditions, the level of the heat, q, is chosen at a slightly above the dynamic-recrystallized temperature which depends also on the type of welding metal.

III. Description of FSW Joints

As mentioned in Section II that a unique onion ring structure was formed due to the three movements of the material under stir welding as shown in Fig. 1. As another description of the stir region, the welding joints shows four distinct zones from the center of the region outward to the edge: nugget zone (NG), thermo-mechanical affected zone (TMAZ), heat-affected zone (HAZ), and base metal (BM) as described in Fig. 3. The most important factor in distinguishing these zones is the type of material flow. HAZ and, to a certain extent, BM zone are characterized by undeformed and coarsening grains, TMAZ experiences mild flow material and elongated grains, and NZ is characterized by fine grains supposedly that they were formed as a result of recrystallization equiaxed fine grains [15].

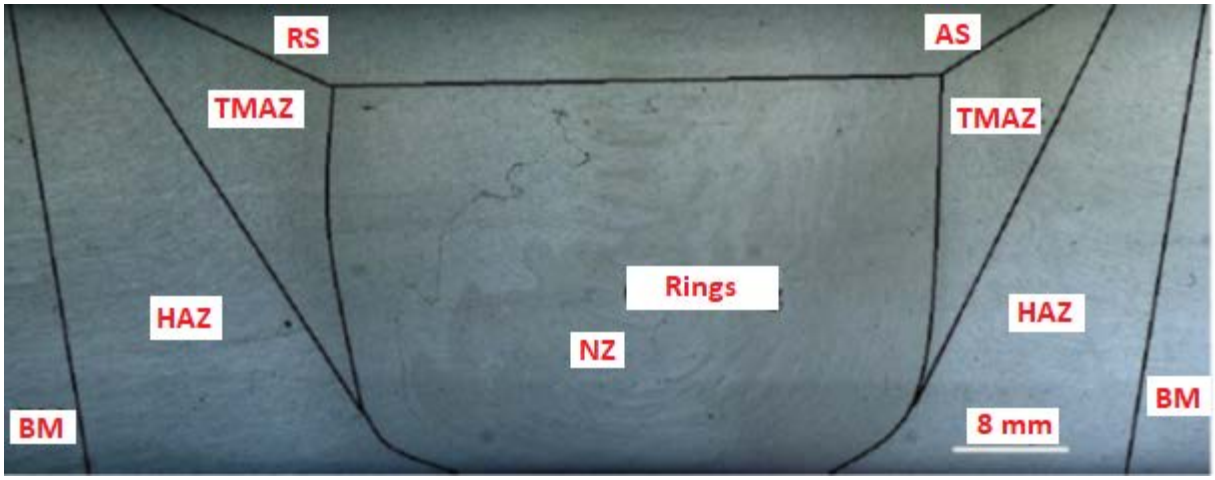

Fig. 3 The structure of FSW joint shows TMAZ, HAZ, NZ, and BM zones [15

IV. Materials and Experiments

A. Chemical composition of AA6061-T6

The alloy used in this report is AA6061-T6 whose chemical composition experimented by ARL Spectrometer and the results are shown in Table I. The weight percentage of the aluminum is 96.9% as measured by ARL Spectrometer. The wt.% of aluminum is deviated from the standard vales [26] by insignificant difference.

Table I. Chemical composition of AA6061-T6

Elements w%	Si	Fe	Cu	Mn	Mg	Cr	Zn	Al
ARL Measurements	0.7	0.5	0.2	0.11	1.1	0.28	0.22	96.9
Standard Values	0.4-0.8	Max 0.7	0.15-0.4	Max 0.15	0.8-1.2	0.04-0.35	Max 0.25	97.9-96.2

B. FSW Setup

FSW process was prepared by the computerized Bridgeport machine shown in Fig. 4. The machine is equipped with a taper-1° threaded tool. The welding was performed by steel T2 whose cylindrical pin is 4.8 mm diameter, length of 4.5 mm, and its shoulder is 20 mm diameter. The

welding parameters are taken at a velocity of 1000 rpm and welding speed rate of 20 mm/min. The specimen was cut at 15*15*3 mm in accordance with ASTM G 71-30 standard. The welding joint parameters were taken at a current of 170 A, voltage 25 V, rod of diameter 3 mm, welding speed rate of 120 mm/min and gas flow of 20 *l*/min. The total number of the identical specimen cut from the NZ region was 36 samples divided into 12 samples of each of the following areas of 200, 400, and 600 mm^2.

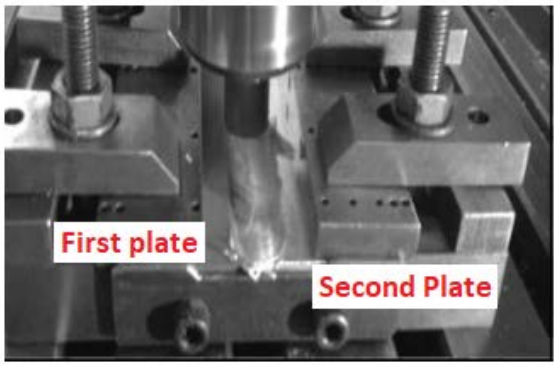

Fig. 4 Bridgeport Friction stirs welding machine

C. FSW Macrostructure

The cross-sectional samples were prepared with three steps: ground, polish, and etching before the samples was tested under an optical microscope purchased from Nikon ME-600 optical microscope provided with a NIKON camera, DXM-1200F. For grinding, SiC paper of diamond paste size of 220, 320, 500, and 1000 was used first and then cleaned with water and alcohol and then dried in air. Polishing was performed by diamond paste paper of 1 μm and special cloth. The third step, etching, a Keller' reagent solution of 94 mils distilled water, 2.5 ml HNO_3, 1.5 ml HCl, and 1 ml HF was used. Samples were then washed with water and oven-dried. Fig. 5 shows the microstructure of FSW zones. It is clear that NZ is the smoother zone amongst the four zones. The BM zone has regular shape since no welding took place in this region.

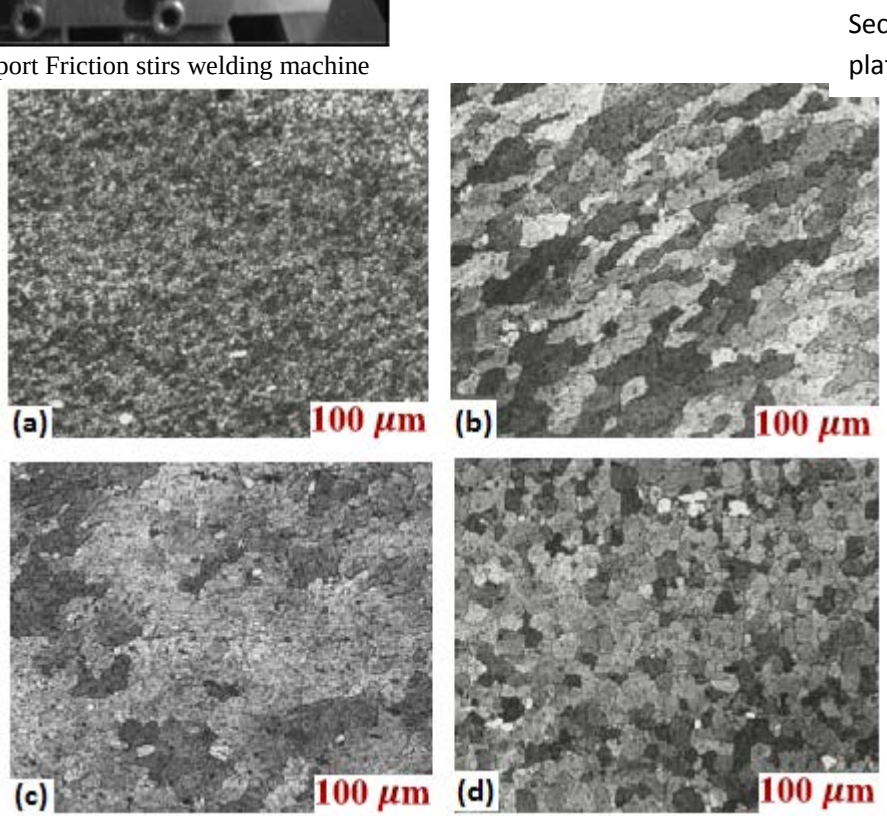

Fig. 5 The zones of AA6061-T6 (a) Nugget Zone, (b) TMAZ, (c) HAZ, and (d) Base Metal

D. Hardness

The hardness of a different zone from the centerline is shown in Fig. 6. The top surface of AA6061-T6 shows asymmetrical behavior from the center of the sample and outward caused by the movement of the plastic-flow in the two sides [27]. The distortion energy as depicted by (1) causes an increase in the strain-hardness uniformity. The hardness has a

minimum amount of 82 HV and 86 HV which are obtained in the HAZ region on the other sides of the centerline. At these two locations, the specimen experienced minimum values that make the sample susceptible to fracture easily. The maximum values of the hardness of 105 HV and 108 HV appear in BM area about 50 mm from the centerline where there is no effect of the stirring power. The hardness in NZ region shows lower hardness than TMAZ region in agreement with the finding of Hall-Petch [28]. This result suggests that the amount of distortion caused by the stirring heat in NZ region is less than the deformation in TMAZ region. The grain size of the four zones as shown in Fig. 5 also plays an important role in the process based on the mechanism presented by Hall-Petch [29]. The results presented are in agreement with the results presented in [27]. Further, the hardness, as well as the mechanical and tensile strength were investigated and there is similarity at different levels were found with the present work [30]-[31].

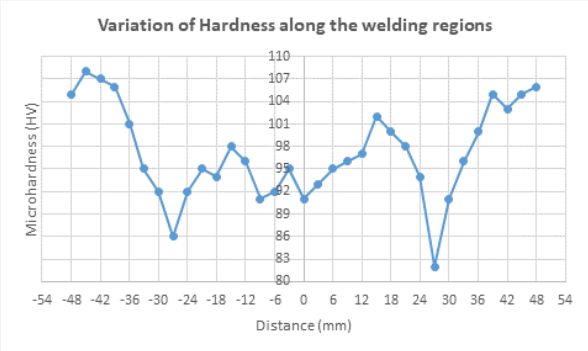

Fig. 6 The hardness of the different zones measured from the centerline

E. Corrosion Tests

The corrosion test implies first the measurement of open circuit potential (OCP) for its use to standardize the sweep measurements. OCP was found at -650 mV and the sweep voltage was taken from 100 mV to +100 mV at a rate of 10 mV/s. The equipment for corrosion test which is shown in Fig. 7 manufactured by WENKING Mlab, Bank Electronic-Intelligent control GmbH, Germany 2007. To perform the corrosion test, AA6061-T6 was used as a working reference electrode immersed in the salt solution. The media speed was controlled by a suitable rotating magnetic field and it was set at the following slurry velocity of 1, 2, and 3 m/s. The technique used is performed by polarization to measure the current density and the voltage. The linear trend of the voltage-current characteristics is linear is used to calculate the corrosion current density (I_{corr}) [32]. The samples were chosen with an area of 0.25 cm2 at TMAZ and HAZ regions exposed to the solution of 3.5% NaCl at TMAZ and HAZ regions.

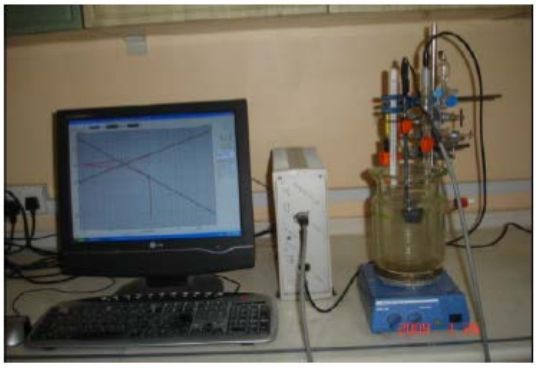

Fig. 7 WENKING MLab corrosion unit

The surface of AA6061-T6 is oxidized due to exposure to air, water, or specific solutions that contain chloride ion [33]. In addition to this dependency, the corrosion rate depends on the heterogeneity of the microstructure of the surface. The aluminum surface shows a passive oxide film due to the exposure to the chloride solution which contains chloride ion. The corrosion test was carried out by cyclic polarization on the NZ-FSW welded sample by choosing three areas of 200, 400, and 600 mm^2 at three speeds of 1, 2, and 3 m/s. The results of the corrosion material removed from the sample were recorded in Table II after 24, 48, 72, and 96 h. Despite the fact that the corrosion test by cyclic polarization was occasionally used, the methodology of assigning specific areas at different zone is a new technique. The impact of the corrosion on the different areas was tested

Table II: corrosion results

Corrosion Time (h)	Area 200 (mm^2)			Area 400 (mm^2)			Area 600 (mm^2)		
	Corrosion (gm/mm^2)*10^{-6}			Corrosion (gm/mm^2)*10^{-6}			Corrosion (gm/mm^2)*10^{-6}		
	Slurry Speed (m/s)			Slurry Speed (m/s)			Slurry Speed (m/s)		
	1	2	3	1	2	3	1	2	3
24	0.47	0.94	2.34	0.96	1.42	3.75	1.75	2.23	5.23
48	0.85	2.24	4.75	1.67	3.65	7.56	3.03	6.83	10.94

72	1.75	4.44	6.18	3.84	7.45	9.45	6.04	12.48	13.45
96	2.67	6.54	9.05	5.86	10.58	12.85	10.34	14.87	21.37

The microscope images were taken by NIKON camera, DXM-1200F for the NZ AA-60613-T6 were presented in Fig. 8. The size of the holes caused by the corrosion increases as the time of corrosion increases which suggests more material is being removed from the surface.

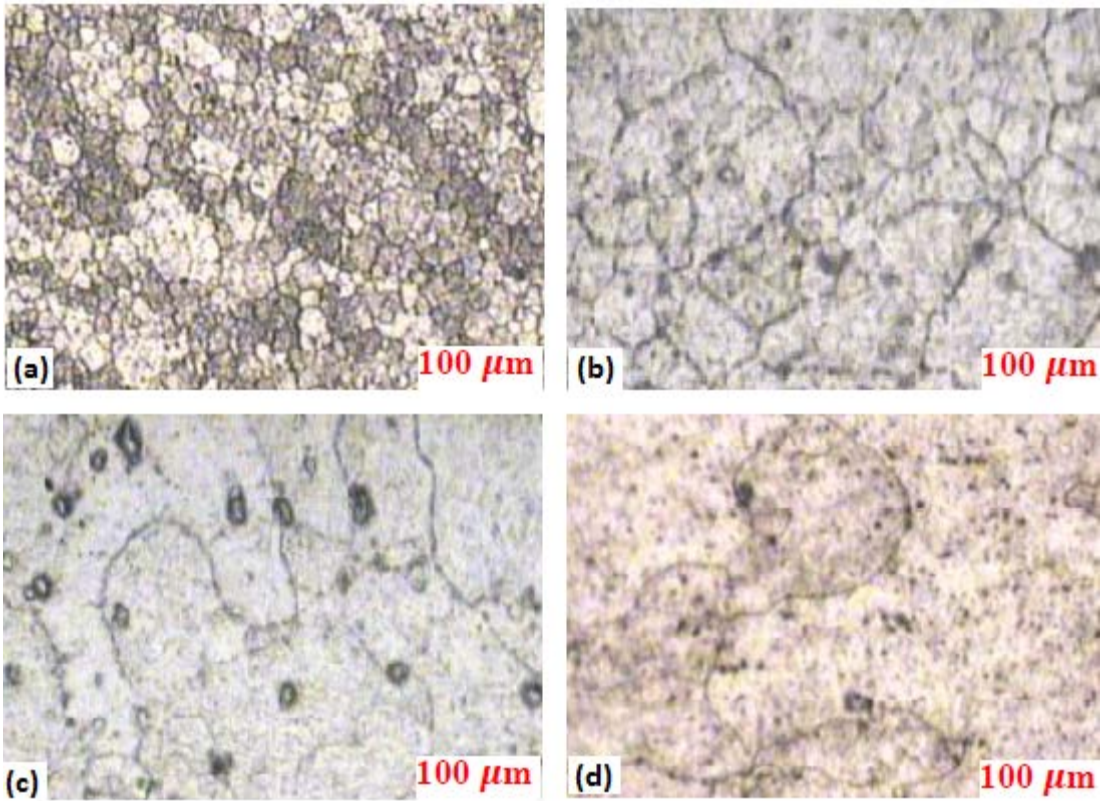

Fig. 8 The NZ of AA6061-T6 after corrosion test (a) 24 h, (b) 48 h, (c) 72 h, and (d) 96 h

The graphical analysis of the corrosion of AA6061-T6 is presented in Fig. 9. When an area of the NZ region of 200, 400, 600 mm^2 was exposed to the solution, the amount of the material removed for any speed increases as the exposing time of the aluminum alloy increases from 24 h to 96 h. The mathematical relation is not linear but it seems to get less amount as the time increases from one day to four days.

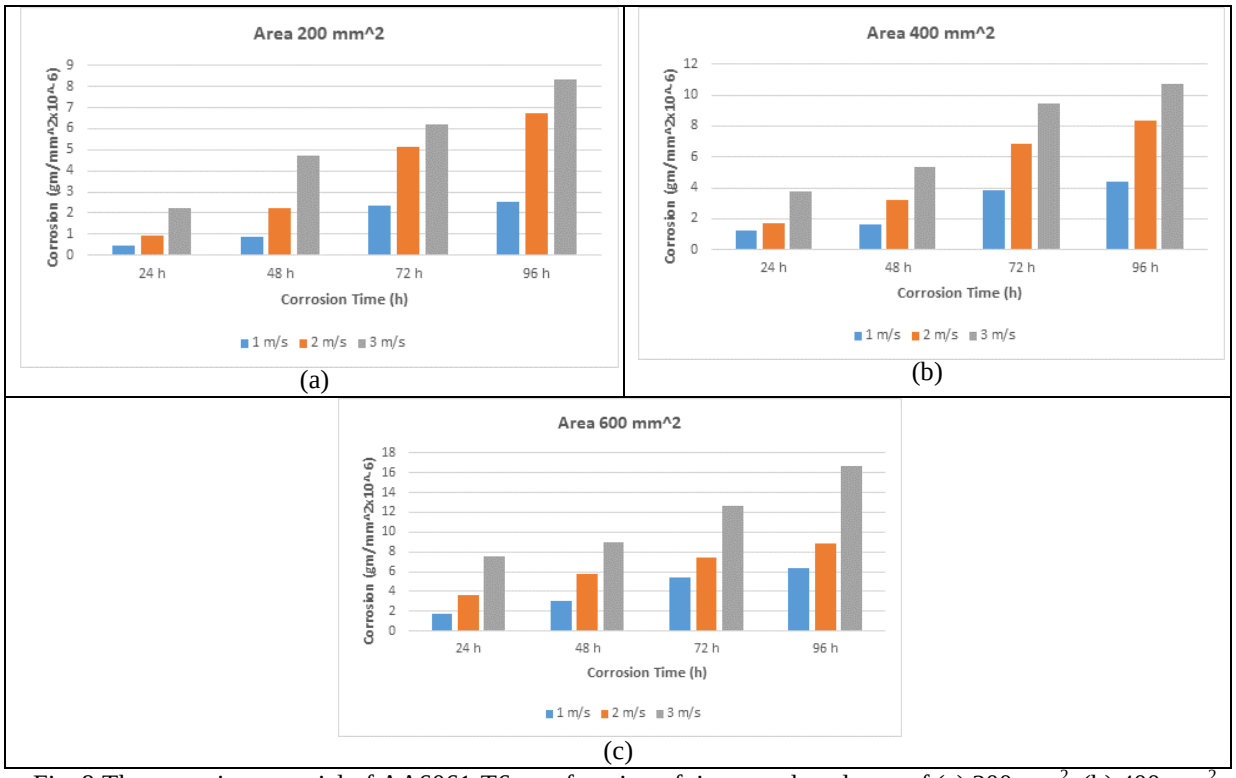

Fig. 9 The corrosion material of AA6061-T6 as a function of time, seed, and area of (a) 200 mm^2, (b) 400 mm^2, and (c) 600 mm^2

To have a mathematical idea about the effect corrosion time, the amount of the AA6061-T6 removed was plotted in Fig. 10 at three speeds of 1, 2, and 3 m/s. The following three fitting equations were obtained:

Table III: Fitting equations of the corrosive material

The fitting Equation	Correlation coefficient (R^2)	Speed (m/s)
$y = 0.4058x^2 - 0.2575x + 0.8692$	0.9978	1
$y = -0.0425x^2 + 3.3404x - 1.8942$	0.9936	2
$y = 0.1883x^2 + 2.4477x + 1.3783$	0.9802	3

The three equations presented in Table III show that the correlation coefficient is very high. The trend of the variation of the corrosion amount is not a linear relationship; it is rather a quadratic relation. The corrosion amount lows down as the time of exposure increases and, possibly, could reach a saturation level after several days. The behavior of the carrion material from AA6061-T6 is similar to that behavior experimented by [34]. It can be noticed that the amount of material in the current study is higher than what was shown in that work due to at least three reasons. The first reason is that of the slurry speed used in this experiment is higher than the slurry speed presented by [34]. The second possible reason is the choice of the zone. In both studies the NZ region as used; however, the exact region of a certain area may play an important role in the results. The NZ region is very wide compared to other regions and determines its exact borders cannot be the same from a study to another study. Thirdly, it widely accepted that the FWS process itself is very complicated and depends on several factors ranging from the expertise of the operator to the manufacturers of AA6061-T6 in regards to the exact composition of the aluminum alloys under investigation. The mathematical analysis as shown in Table III and the subsequent graphs in Fig. (10) is used for the first time and may be considered as one of the particulars of the research in this paper.

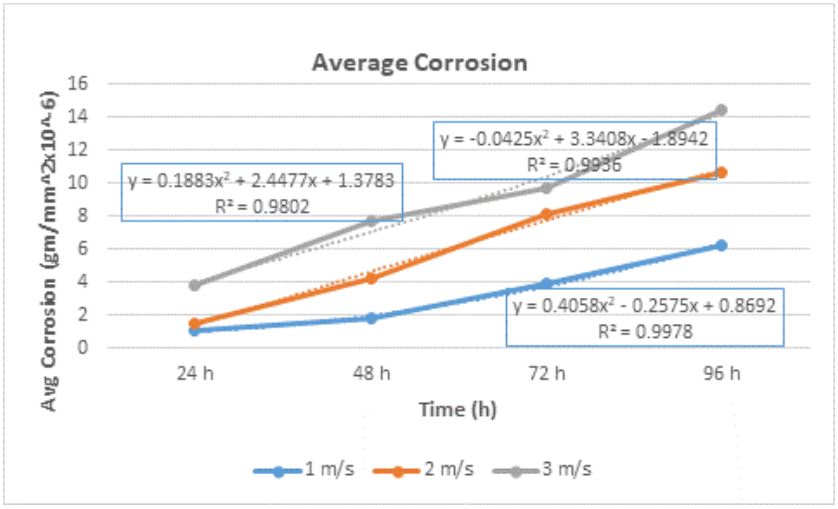

Fig. 10. Average corrosion as a function of slurry speed and exposure corrosion time

Fig. 11 shows three modes of variation of the corrosion amount as a function of area of 200, 400, 600 mm2 (Fig. 11 a), slurry speed of 1, 2, and 3 m/s (Fig. 11 b), and finally as a function of exposure time of 24, 48, 72, and 96 h (Fig. 11 c). The amount of exposure material increases as the area, slurry speed, and exposure time increase.

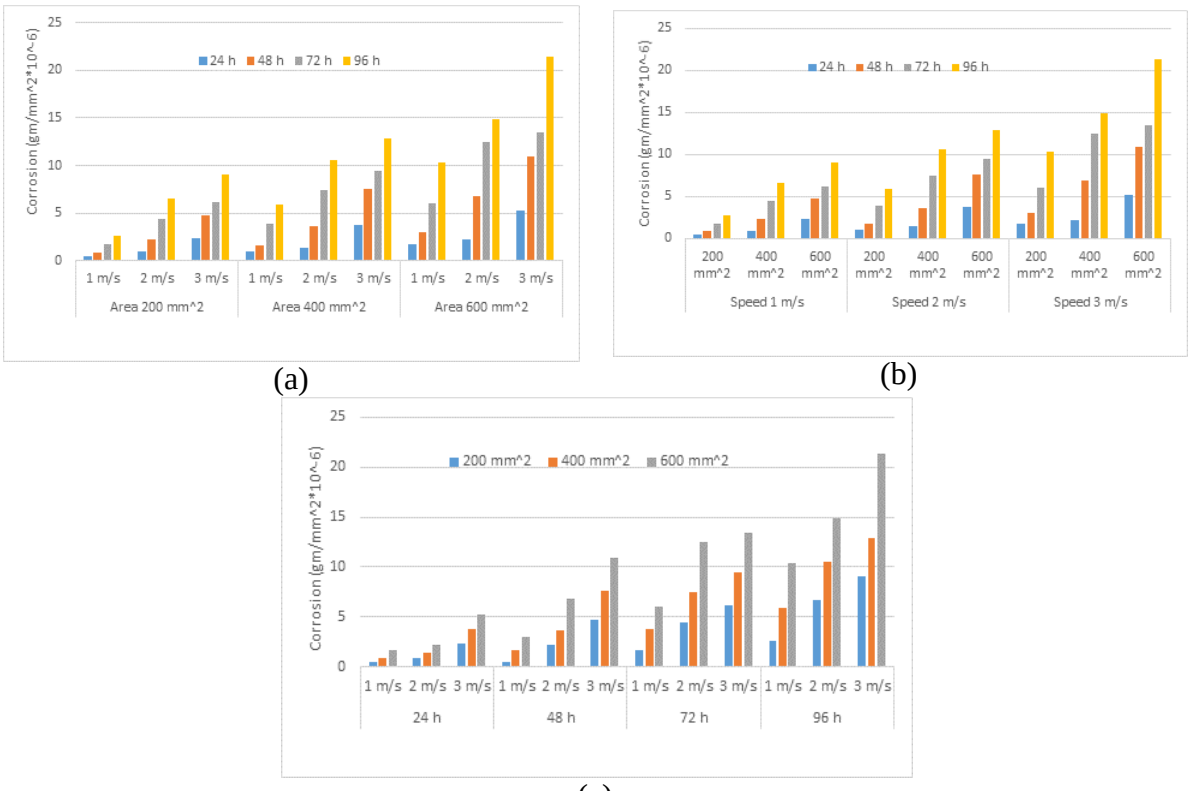

Fig. 11 Influence of the four factors of area, slurry speed, and exposure time on corrosion

The relative amount of the corrosion material for all areas of 200, 400, and 600 mm^2 and at a different slurry speed of 2 m/s, the relative corrosion amount is the highest compared to the speed of 1 m/s and 3

m/s. One possible reason for this finding could be as a result of the flow of slurry is more effective at this speed compared to other two slurry speeds. Moreover, the relative amount of corrosion at an exposure time of 48 h shows the highest amount at any speed or any surface. These results suggest that the effect of the corrosive solution is highest after 48 h and beyond that, the effect of the solution declines.

V. Conclusion and future Challenges

In the engineering field, the use of aluminum alloys is very critical to the industry and the demand to weld two or more parts is very common in the industry. FSW has been widely used in aluminum welding because it is convenient, inexpensive, and environmentally friendly. The corrosion caused by an external agent plays an important role in the limitation of the aluminum alloys. In addition to testing the surface of AA6061-T6 by optical microscope, the corrosion in seawater of the selected region from NZ was investigated at 24, 48, 72, and 96 h, with slurry speed of 1, 2, 3 m/s, using three surface areas of 200, 400, and 600 mm^2. The results suggest that increasing the slurry velocity and corrosion time will cause more removal material from the ZN region of the AA6061-T6 alloy. However, the most effective exposure time appears after 48 h and the most effective slurry speed is 2 m/s.

For future explorations, it is expected that the mechanical properties could be improved as a result of adopting appropriate process parameters such as the slurry speed, optimizing the mixing process of the aluminum alloy, and the evaluation of microstructure evolution of Al-alloy series. The second issue of possible future work is how to handle the decreasing of the mechanical strength of TMAZ and SZ. In this regards, the dominant factors that result in decreasing of the mechanical strength should be identified in order to enhance the mechanical properties. Finally, the microstructure of the Al alloys depends on the flow of plasticized material due to the rotational speed and the applied pressure. A future possible work may deal with the improving the microstructure of the Al alloy by optimizing these parameters.

Acknowledgement:

The experimental work was supported the Institute of Technology, Baghdad, Iraq under the grant No 0012-IoT-2017-2-11 which is a part of the support to the academic personnel in order to achieve better qualifications.

References

[1] V. K. Patel, S. D. Bhole, D. L. Chen. (2011). “Influence of ultrasonic spot welding on microstructure in a magnesium alloy”. Scr. Mater. vol. 65, pp.911–914.

[2] A. Heinz, A. Haszler, C. Keidel, S. Moldenhauer, R. Benedictus, W.S.Miller. (2000). “Recent development in aluminium alloys for aerospace applications” Journal of Materials Science and Engineering A, vol. 280, issue 1, pp 102-107.

[3] N. Jin, H. Zhang, Y. Hay, W. X. Wu, J. H. Chen. (2009). “Hot deformation behavior of 7150 aluminum alloy during compression at elevated temperature” Journal of Materials Characterization. vol. 60, issue 6, pp. 530-536.

[4] I. Zhen, H. Hu, X. Wang, B. Zhang, W. Shao. (2009). “Distribution characterization of boundary misorientation angle of 7050 aluminum alloy after high-temperature compression.” Journal of Materials Processing Technology. vol. 209, issue 2, pp. 754-761.

[5] J. Sarkar, Y. Prasad, M. Surappa. (1995). “Optimization of hot workability of an Al-Mg-Si alloy using processing maps.” Journal of Journal of Materials Science. vol. 30, issue 11, pp. 2843-2848.

[6] G. Z. Quan, B. S. Kang, T. W. Ku, W. J. Song, W. J. (2011). “Identification for the optimal working parameters of Al-Zn-Mg-Cu alloy with the processing maps based on DMM.” The International Journal of Advanced Manufacturing Technology. vol. 56, issue 9, 1069-1078.

[7] S. Y. Yu, X. J. Chen, Z. Q. Huang, Z.Q., Y. H. Liu. (2010). “Microstructure and mechanical properties of friction stir welding of AZ31B magnesium alloy added with cerium.” J. Rare Earths. vol. 28, pp. 317–320.

[8] Z. Y. Ma, A. L. Pilchak, M. C. Juhas, J. C. Williams. (2008). “Microstructural refinement and property enhancement of cast light alloys via friction stir processing.” Scr. Mater. vol. 58, pp. 361–366.

[9] S. H. Chowdhury, D. L. Chen, S. D. Bhole, X. Cao, P. Wanjara. (2013). “Friction stir welded AZ31 magnesium alloy: Microstructure, texture, and tensile properties.” vol. Metall. Mater. Trans. A. 44, pp. 323–336.

[10] D. J. Liu, R. L. Xin, L. Z. Zhao. (2017). “Effect of textural variation and twinning activity on fracture behavior of friction stir welded AZ31 Mg alloy in bending tests.” J. Alloys Compd. vol. 93, pp. 808–815.

[11] O. S. Salih, H. Ou, W. Sun, D. G. McCartney. (2015). “A review of friction stir welding of aluminium matrix composites.” vol. Mater. Des. pp. 86, 61–71.

[12] W. M. Thomas, D. J. Staines, I. M. Norris.(2003). “Friction stir welding tools and developments.” Weld. World vol. 47, pp 10–17.

[13] R.De A. H. K. D. H. Bhadeshia, T. Debroy. (2011). “Review: Friction stir welding tools.” Sci. Technol. Weld. Join. vol. 16, pp 325–342.

[14] Y. N. Zhang, X. Cao, S. Larose, P. Wanjara. (2012). “Review of tools for friction stir welding and processing.” Can. Metall. Q. vol. 51, pp 250–261.

[15] L. Yajie, Q. Fengming, L. Cuirong, W. Zhisheng. (2017).” A Review: Effect of Friction Stir Welding on Microstructure and Mechanical Properties of Magnesium Alloys.” Metals, Metals vol. 7, pp 524-538.

[16] M. N. Avettand-Fènoël, A. Simar. (2016). “A review about friction stir welding of metal matrix composites.” Mater. Charact. vol. 120, pp 1–17.

[17] R. Nandan, T. DebRoy, H. K. D. H. Bhadeshia. (2008). “Recent advances in friction-stir welding process, weldment structure and properties.” Prog. Mater. Sci. vol. 53, pp 980–1023.

[18] Q. Yang, S. Mironov, Y. S. Sato, K. Okamoto. (2010). "Material flow during friction stir spot welding." Mater. Sci. Eng. A vol. 527, pp 4389–4398.
[19] P. Su, A. Gerlich, T. H. North, G. T. Bendzsak. (2007). "Intermixing in dissimilar friction stir spot welds." Metall. Mater. Trans. A. vol. 38, pp 584–595.
[20] S. Rajakumar, A. Razalrose, V. Balasubramanian. (2013). "Friction stir welding of AZ61A magnesium alloy." Int. J. Adv. Manuf. Technol. vol. 68, pp 277–292.
[21] W. B. Lee, Y. M. Yeon, S. B. Jung. (2004). "Mechanical properties related to microstructural variation of 6061 Al alloy joints by friction stir welding. Mater. Trans. vol. 45, pp 1700–1705.
[22] X. He, F. Gu, A. Ball. (2014). "A review of numerical analysis of friction stir welding." Prog. Mater. Sci. vol. 65, pp 1–66.
[23] P. Ulysse. (2002). "Three-dimensional modeling of the friction stir-welding process." Int. J. Mach. Tools Manuf. vol. 42, pp 1549–1557.
[24] P. Heurtier, M. J. Jones, C. Desrayaud, J. H. Driver, F. Montheillet, D. Allehaux. (2006). "Mechanical and thermal modelling of friction stir welding." J. Mater. Process. Technol. vol. 171, pp 348–357.
[25] Y. S. Sato, H. Kokawa. (2000). "Distribution of tensile property and microstructure in friction stir weld of 6063 aluminum." Metall. Mater. Trans. A vol. 32, pp 3023–3031.
[26] ASM (1992). Metals Handbook, Vol.2 - Properties and Selection: Nonferrous Alloys and Special- Purpose Materials, ASM International 10th Ed.
[27] W. Xu, J. Liu, G. Luan, C.Dong. (2009). "Temperature evolution, microstructure and mechanical properties of friction stir welded thick 2219-O aluminum alloy joints," Materials & Design. vol. 30, pp 1886-1893.
[28] D. H. Jeong, U. Erb, K. T. Aust, G. Palumbo. (2003). "The relationship between hardness and abrasive wear resistance of electrodeposited nanocrystalline Ni–P coatings," Scripta Materialia. vol. 48, pp 1067-1072.
[29] Y. S. Sato, S. Park, H. Kokawa. (2001). "Microstructural factors governing hardness in friction-stir welds of solid-solution-hardened Al alloys." Metall and Mat Trans A, vol. 32, pp 3033-3042.
[30] H. B. Chen, Y. Keng, L. Tao, S. B. Chen, Y.J. Cheng, Z. Yong. (2006). "The investigation of typical welding defects for 5456 aluminum alloy friction stir welds. Material science and engineering" vol. 433, pp 64-69.
[31] Y. M. Hwang, Z. W. Kang, Y. C. Chiou, H. H. Hsu. (2008). "Experimental study on temperature distributions within the work piece during friction stir welding of aluminum alloys." Int. J. of Machine Tool and Manufacturing." vol. 48, pp 778-787.
[32] D. G. Enos. (1997). "The Potentiodynamic Polarisation Scan,." Technical Report 33, University of Virginia.
[33] K. R. Trethewey, J. Chamberlain. (1996). "Corrosion for Science and Engineering" Longman Group Limited, 2nd Edition.
[34] O. M. Irfran, H. M. Omar. (2017). "Experimental Study and Prediction of Erosion-Corrosion of AA6066 Aluminum Using Artificial Neural Network." International Journal of Mechanical & Mechatronics Engineering IJMME-IJENS vol. 17, issue 06, pp 17-31.

K. M. Jawad became a member in NAUN in 2018. He was born in Bagdad/Iraq where he finished his primary and undergraduate studies. He received his graduate degree from Belgrade University in Mechanical Engineering in 1985. He, since then is working in the Middle Technical University. He is active in welding technology. He attended several conferences and authored publication at local and international levels.